Pressure effects in supercooled water: comparison between a 2D model of water and experiments for surface water on a protein

Giancarlo Franzese[1]**, Kevin Stokely**[2]**, Xiang-qiang Chu**[3]**,
Pradeep Kumar**[2,4]**, Marco G Mazza**[2]**, Sow-Hsin Chen**[3] **and
H Eugene Stanley**[2]

[1] Departament de Física Fonamental, Universitat de Barcelona, Diagonal 647,
08028 Barcelona, Spain
[2] Center for Polymer Studies and Department of Physics, Boston University, Boston,
MA 02215, USA
[3] Department of Nuclear Science and Engineering, Massachusetts Institute of Technology,
Cambridge, MA 02139, USA
[4] Center for Studies in Physics and Biology, Rockefeller University, New York,
NY 10021, USA

E-mail: gfranzese@ub.edu

Abstract
Water's behavior differs from that of normal fluids, having more than sixty anomalies. Simulations and theories propose that many of these anomalies result from the coexistence of two liquid phases with different densities. Experiments in bulk water confirm the existence of two local arrangements of water molecules with different densities, but, because of inevitable freezing at low temperature T, cannot ascertain whether the two arrangements separate into two phases. To avoid the freezing, new experiments measure the dynamics of water at low T on the surface of proteins, finding a crossover from a non-Arrhenius regime at high T to a regime that is approximately Arrhenius at low T. Motivated by these experiments, Kumar *et al* (2008 *Phys. Rev. Lett.* **100**, 105701) investigated, by Monte Carlo simulations and mean field calculations on a cell model for water in two dimensions (2D), the relation of the dynamic crossover with the coexistence of two liquid phases. They show that the crossover in the orientational correlation time τ is a consequence of the rearrangement of the hydrogen bonds at low T, and predict that: (i) the dynamic crossover is isochronic, i.e. the value of the crossover time τ_L is approximately independent of pressure P; (ii) the Arrhenius activation energy $E_A(P)$ of the low-T regime decreases upon increasing P; (iii) the temperature $T^*(P)$ at which τ reaches a fixed macroscopic time $\tau^* \geqslant \tau_L$ decreases upon increasing P; in particular, this is true also for the crossover temperature $T_L(P)$ at which $\tau = \tau_L$.

Here, we compare these predictions with recent quasi-elastic neutron scattering (QENS) experiments performed by Chu *et al* on hydrated proteins at different values of P. We find that the experiments are consistent with these three predictions.

(Some figures in this article are in colour only in the electronic version)

1. Introduction

Water has many anomalies in comparison to normal liquids [1]. Experiments show that its thermodynamics fluctuations and response functions, such as the isobaric specific heat C_P or the magnitude of the isobaric thermal expansion coefficient α_P, increase when temperature is decreased [2]. These anomalies are more pronounced in the supercooled liquid state, below $0\,°C$. This state, metastable with respect to ice, can be observed at temperatures as low as $-47\,°C$ in plants [3], $-41\,°C$ in laboratory at atmospheric pressure [4] and $-92\,°C$ at 2 kbar [5].

The anomalies have been interpreted on the basis of models that propose different scenarios. The scenarios can be divided into two main categories: (a) those scenarios that include the coexistence at low T of two liquids with different densities, and (b) a scenario in which water forms local regions of different densities, but does not separate into two phases.

1.1. Scenarios with coexistence of two liquids

The liquid–liquid critical point scenario. In 1992 Poole *et al* [6], on the basis of molecular dynamic simulations for ST2- and TIP4P-water, proposed that supercooled water separates into two liquid phases with different densities below 200 K and above 150 MPa. The low-density liquid (LDL) and the high-density liquid (HDL) form of water coexist along a first-order phase separation line with negative slope in the pressure–temperature P–T phase diagram and terminate in a liquid–liquid critical point (LLCP). The LLCP scenario has been confirmed by simulations with various water models [7].

The occurrence of the LLCP has been rationalized with different theoretical models by assuming (a) the anticorrelation between energy and volume in the H (hydrogen) bonds formation and (b) the possibility of forming different kinds of H bonds. An example is the thermodynamic free energy model of Poole *et al* that hypothesizes the formation of strong H bonds when a geometrical condition on the molar volume is satisfied [8].

Another example is the microscopic cell model introduced in [9, 10] and studied in detail in [11, 12], in which the correlation between the H bonds, due to the O–O–O interaction, is incorporated. In this model the liquid–liquid (LL) phase transition is due to the tetrahedral ordering at low T and P of the H bonds, as explained in the following section.

The LLCP is predicted to lie in a region of the P–T phase diagram where the freezing of bulk water is inevitable. Therefore, direct experimental verification of the LLCP scenario is challenging. However, Soper and Ricci in 2000 showed with neutron diffraction measurements that the local arrangement of water molecules changes up to the second shell, increasing the local density when P is increased from 26 to 400 MPa at $-5.15\,°C$ [13]. This structural change was initially observed by varying T from about 263 to 313 K in x-ray structure factor experiments for heavy water D_2O in 1983 [14]. The data show that by decreasing T the average O–O–O angle increases toward the tetrahedral angle 109.47° [14]. This result has been reaffirmed by Ricci *et al* in a recent experiment [15].

The critical point free scenario. Another scenario that hypothesizes a liquid–liquid (LL) phase transition has been considered recently [16]. In this scenario the LL first-order phase transition extends to negative P and merges the liquid spinodal, but without a critical point. A rationalization of this scenario has been recently proposed on the basis of the microscopic cell model for water [9, 17], showing that this scenario has a liquid spinodal that reenters from negative to positive P [17].

The stability limit scenario. The reentrant spinodal discussed in [17] was earlier proposed in the stability limit scenario [18] as the origin of the anomalies of water. Although in the initial formulation of the stability limit scenario the occurrence of the LL phase transition was not hypothesized, it was successively introduced for thermodynamic consistency [19] and found also in the thermodynamic free energy model of Poole *et al* [8].

1.2. Scenario without coexistence of two liquids

The singularity free scenario. This scenario assumes that the H-bonds linking molecules are uncorrelated. Under this hypothesis, water anomalies are the effect of the negative volume-entropy cross fluctuations [20, 21] and the large increase of response functions seen in the experiments only represents an apparent singularity, due to local density fluctuations. The regions with different local density do not form separate phases. A pressure increase gives rise to a sharp, but continuous, increase of density, as in the supercritical region of the LLCP scenario. The continuous structural change is found also in *ab initio* water simulations [22] at very high pressure, $P = 10^4$ MPa, and $T = 600$ K. This scenario is recovered by the microscopic cell model [9] in the limiting case of no cooperativity among the H bonds.

The singularity free scenario, in the region accessible by experiments, reproduces the same phase diagram as the scenarios with coexistence of two liquids. Therefore, it is interesting to understand if there are observable differences among these scenarios. In particular, recent experiments and simulations, described in the next sections, have analyzed the case of the dynamics of water surrounding proteins or confined in nanopores, interpreting the experimental results within the context of the different scenarios.

2. Hydrated proteins

Recent experiments on surface water and water hydrating proteins [23–25] have shown that liquid water exists at temperatures as low as $-113\,°C$ [26] at ambient pressure. At these extremely low temperatures interesting dynamical phenomena occur [27–30], suggesting a possible relation for the dynamics of the biological macromolecules with that of the surrounding water [25, 31].

At low T, proteins exist in a ('glassy') state with no conformational flexibility and with very low biological activity. For hydrated proteins above about 220 K, the flexibility is restored, allowing the sampling of more conformational sub-states. Hence, the protein becomes biologically active at these

temperatures. This dynamical transition is common to many biopolymers and is believed to be triggered by the strong coupling with the mobility of the hydration water [28], which shows a similar dynamical transition at about the same T [23]. Chen *et al* by studying the translational correlation time of water molecules hydrating a lysozyme protein [23], DNA [32] and RNA [33], found that at about 220 K the dynamics of hydration water changes from non-Arrhenius at high T to Arrhenius at low T. By definition a correlation time τ has an Arrhenius behavior when

$$\tau = \tau_0 \exp[E_A/k_B T] \tag{1}$$

where τ_0 is the correlation time in the high-T limit, E_A is a T-independent activation energy and k_B is the Boltzmann constant. On the other hand, τ is non-Arrhenius when its behavior cannot be fitted with the expression in equation (1).

Motivated by these experiments, Kumar *et al* [34] simulated, using the TIP5P model, the dynamics and thermodynamic behavior of hydration water for (i) an orthorhombic form of hen egg-white lysozyme and (ii) a Dickerson dodecamer DNA at constant pressure $P = 1$ atm, several constant temperatures T, and a constant number of water molecules N. Kumar *et al* [34] found that the mean square fluctuations $\langle x^2 \rangle$ of the biomolecules changes its functional form below $T_p \approx 245$ K, for both lysozyme and DNA. They also found that the specific heat C_P of the different system (biopolymer and water) displays a maximum at $T_W \approx (250 \pm 10)$ K for both biomolecules.

To describe the quantitative changes in structure of hydration water, Kumar *et al* [34] calculated the local tetrahedral order parameter Q [35] for hydration water surrounding lysozyme and DNA, and found that the rate of increase of Q has a maximum at $T_Q = (245 \pm 10)$ K, the same temperature as the crossover in the behavior of mean square fluctuations. Finally, they found that the diffusivity of hydration water exhibits a dynamic crossover from non-Arrhenius to Arrhenius behavior at the crossover temperature $T_\times \approx (245 \pm 10)$ K for lysozyme and $T_\times \approx (250 \pm 10)$ K for DNA. Note that $T_\times$ is much higher than the glass transition temperature, estimated for TIP5P as $T_g = 215$ K [7]. Thus this crossover is not likely to be related to the glass transition in water. Therefore, the fact that $T_p \approx T_\times \approx T_W \approx T_Q$ is evidence of the correlation between the changes in protein fluctuations and the hydration water thermodynamics and structure. Before analyzing this relation in more detail it is worth considering the results of experiments about water confined in nanostructures.

3. Confined water

The non-Arrhenius to Arrhenius dynamic crossover has also been found in water confined in 20 Å MCM-41 silica pores. Indeed, in 2004 Faraone *et al* found the crossover for confined water at $T_L \approx 221$ K by studying the structural relaxation time by neutron scattering [36]. This result was reinforced by the neutron magnetic resonance measurements of Mallamace *et al* showing the crossover at $T_L \approx 225$ K for the self-diffusion of confined water [26].

In 2005, Liu *et al* [37] showed that, by increasing the pressure, the dynamic crossover of water confined in 20 Å MCM-41 silica pores disappears at a pressure between 1200 and 1600 bar. Xu *et al* [38], by using simulations of TIP5P, ST2 water and other models for liquids with the LLCP, showed that the disappearance of the dynamic crossover of water could be associated to the presence of the LLCP (C'). Indeed, the simulations for water display the same phenomenology of the experiments, with a crossover in the diffusion coefficient at P below the LL critical pressure $P < P_{C'}$, and with no crossover at $P > P_{C'}$. Xu *et al* [38] presented numerical evidence that the crossover at $P < P_{C'}$ is associated to the structural change occurring at the temperature of the maximum of the specific heat $C_P^{\max}$ along a line departing from the LLCP and extending into the one-phase region of the P–T phase diagram. This line, close to the LLCP, coincides with the Widom line [12], defined as the locus of the maximum correlation length in the one-phase region.

Xu *et al* [38] interpreted the absence of the crossover in the diffusion coefficient at $P > P_{C'}$ as a consequence of the fact that the HDL-to-LDL spinodal occurs at almost constant $P \simeq P_{C'}$ for decreasing T. Therefore, when cooled at $P > P_{C'}$, water never crosses the HDL-to-LDL spinodal and does not undergo the structural change responsible for the dynamic crossover.

Hence, although the origin of the crossover has different interpretations [29], the experimental and numerical evidence suggests that the change in the dynamics is triggered by a local rearrangement of the H-bond network [30]. Experiments and simulations, however, cannot give a definitive answer due to their finite resolution. For this reason it is interesting to analyze the dynamic crossover of supercooled water within the framework of a Hamiltonian cell model that allows simulations and analytic calculations [10, 12].

4. Water model

We consider a cell model for water [9–12] based on the experimental observations that on decreasing P at constant T, or on decreasing T at constant P, (i) water displays an increasing local tetrahedrality [39, 40], (ii) the volume per molecule increases at sufficiently low P or T, and (iii) the O–O–O angular correlation increases [13, 15], consistent with simulations [22, 41].

The system is divided into cells $i \in [1, \ldots, N]$ on a regular lattice, each containing a molecule, with a volume $v_i \geqslant v_0$, where v_0 is the hard-core volume of one molecule, with a total volume $V = \sum_i^N v_i$. In d dimensions the distance between two nearest neighbor (n.n.) molecules i and j is $r_{i,j} \equiv (v_i^{1/d} + v_j^{1/d})/2$. Since v_i is a continuous variable, the distance $r_{i,j}$ is continuous.

Every cell is occupied by a molecule. The dimensionless density for the molecule in cell i is $v_0/v_i \in (0, 1]$. We use a discrete two-state liquid-index n_i to quantify if the cell i is in the liquid phase or not, with $n_i = 1$ if $v_0/v \geqslant 0.5$ and $n_i = 0$ otherwise. Therefore, $\sum_i^N n_i$ is the total number of liquid cells and $N - \sum_i^N n_i$ is the total number of gas cells.

The van der Waals attraction between the molecules is represented by the Hamiltonian term

$$\mathcal{H} \equiv -\epsilon \sum_{\langle i,j \rangle} n_i n_j, \tag{2}$$

where $\epsilon > 0$ is the van der Waals attraction energy, which induces the liquid–gas phase transition.

Each molecule i has four H-bond indices $\sigma_{ij} \in [1, \ldots, q]$, corresponding to four n.n. cells j, giving rise to q^4 different molecular orientations. Directional bonding and intramolecular (IM) interactions are accounted for by, respectively, the two Hamiltonian terms

$$\mathcal{H}_B \equiv -J \sum_{\langle i,j \rangle} n_i n_j \delta_{\sigma_{ij}\sigma_{ji}}, \tag{3}$$

where the sum is over n.n. cells, $0 < J < \epsilon$ is the bond energy, $\delta_{a,b} = 1$ if $a = b$ and $\delta_{a,b} = 0$ otherwise, and

$$\mathcal{H}_{IM} \equiv -J_\sigma \sum_i n_i \sum_{(k,\ell)_i} \delta_{\sigma_{ik}\sigma_{i\ell}}, \tag{4}$$

where $\sum_{(k,\ell)_i}$ denotes the sum over the IM bond indices (k, l) of the molecule i and $J_\sigma > 0$ is the IM interaction energy with $J_\sigma < J$, which models the angular correlation between the bonds on the same molecule.

When H bonds are formed, a small volume v_B is added to the local volumes v_i and v_j of the two H-bonded molecules i and j, increasing their average distance to $r_{ij} \equiv (v_i^{1/d} + v_j^{1/d} + v_B^{1/d})/2$. Pictorially, this can be viewed as a local increase of the excluded volume associated with molecules i and j and is consistent with the experimental observation that H-bonded molecules form a low-density open structure. Therefore, the total volume is proportional to the total number N_B of H bonds, as

$$V \equiv V_0 + N_B v_B, \tag{5}$$

where $V_0 \equiv N v_0$ is the volume of the liquid with no H bonds, and

$$N_B \equiv \sum_{\langle i,j \rangle} n_i n_j \delta_{\sigma_{ij},\sigma_{ji}}. \tag{6}$$

Therefore, the cell model has the total Hamiltonian

$$\mathcal{H}_{tot} \equiv \mathcal{H} + \mathcal{H}_B + \mathcal{H}_{IM} \tag{7}$$

with the volume given by equation (5).

5. Thermodynamics of the water model

The cell model described in the previous section has been analyzed by mean field calculations [9–12, 42, 43] and Monte Carlo simulations [11, 42, 43]. The model's parameters considered in these studies are: $J/\epsilon = 0.5$, $J_\sigma/\epsilon = 0.05$, $v_B/v_0 = 0.5$ and $q = 6$.

5.1. Mean field

The mean field results [12], consistent with computer simulations [11], reproduce the known phase diagram of fluid water, with the liquid–gas coexistence region ending in the critical point C, at $k_B T_C/\epsilon = 1.03 \pm 0.03$ and $P_C v_0/\epsilon = 0.18 \pm 0.04$, and with the temperatures of maximum density (TMD) at constant P that decreases with increasing P as in the experiments [49, 50].

In the deeply supercooled region the density has another discontinuity marking the coexistence region between two liquids at different densities. This discontinuity is associated with a discontinuity in m_σ^{min}, the value of the tetrahedral order parameter $m_\sigma \in [0, 1]$ that minimizes the molar Gibbs free energy g. Here, m_σ quantifies the number of H bonds with tetrahedral orientation and is defined as the difference between the number-density of $\sigma_{ij} = 1$ and the average number-density for the other $q - 1$ states, i.e., $m_\sigma \equiv n_\sigma - (1 - n_\sigma)/(q - 1)$, where

$$n_\sigma \equiv \frac{1}{4nN} \sum_{\langle i,j \rangle} n_i n_j \delta_{\sigma_{ij},1} \tag{8}$$

and where the state $\sigma_{ij} = 1$ corresponds to the appropriate state to form a (not bifurcated) H bond with local tetrahedral order.

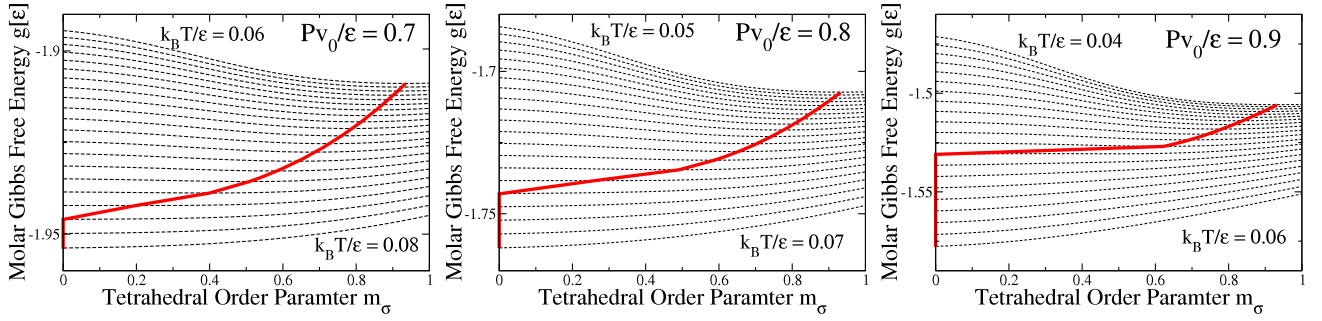In the NPT ensemble, the relevant free energy is the Gibbs energy per mole

$$g \equiv u - Ts + Pv, \tag{9}$$

where u is the molar energy, s the molar entropy, and v the molar volume. As explained in [12], these quantities can all be written in the mean field approximation, giving rise to a mean field expression for g that can be minimized with respect to the gas–liquid order parameter m and the tetrahedral order parameter m_σ.

For any P at low $k_B T/\epsilon < 0.1$, g has its minimum for $m = 1$ (liquid phase value) and for a value m_σ^{min} that changes with T and P (figure 1). At constant P, m_σ^{min} decreases with increasing T, displaying a discontinuity above $Pv_0/\epsilon \simeq 0.8$ (figure 1 right). The discontinuity disappears at $Pv_0/\epsilon \simeq 0.8$ (figure 1 center) and the approach of m_σ^{min} to 0 is always continuous below $Pv_0/\epsilon = 0.8$ (figure 1 left). The appearance of the discontinuity in m_σ^{min} denotes the occurrence at high P of a phase transition between two liquid phases with a different value of the tetrahedral order parameter m_σ: an orientationally disordered phase ($m_\sigma = 0$) at high T, with no tetrahedral order, and a tetrahedrally ordered phase ($m_\sigma > 0.5$) at low T. The phase separation disappears at the liquid–liquid critical point C', that in mean field is estimated at $k_B T_{C'}/\epsilon = 0.062 \pm 0.02$ and $P_{C'} v_0/\epsilon = 0.82 \pm 0.02$ [12]. The discontinuity in m_σ determines the discontinuity in the density between the two phases, as can be shown analytically [12], separating the liquid in LDL at low T and HDL at high T, consistent with the LLCP scenario.

5.2. Monte Carlo

In the Monte Carlo simulations of the cell model, the Hamiltonian $\mathcal{H}_{tot}$ in equation (7) is simulated with the standard spin-flip method [11, 42, 43]. For sake of simplicity, we solve
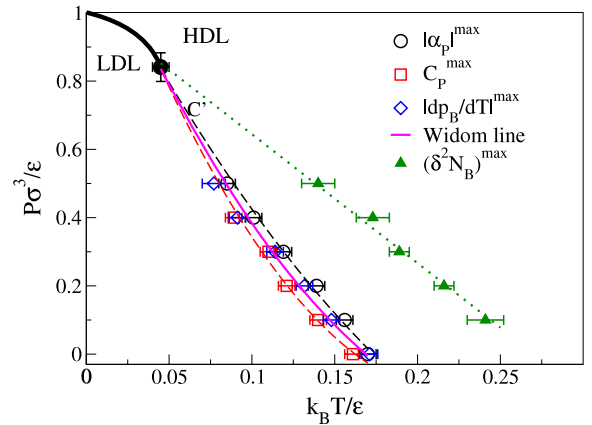
Figure 1. The mean field molar Gibbs free energy g (dashed lines), in units of ϵ, as a function of the dimensionless tetrahedral order parameter $m_\sigma \in [0, 1]$ for different choices of T and P. The thick (red) line connects the points m_σ^{min} of minimum g at different T for $Pv_0/\epsilon = 0.7$ (left panel), 0.8 (center panel), 0.9 (right panel). In each panel the topmost line corresponds to the lowest $k_B T/\epsilon$ (0.06, 0.05 and 0.04, respectively) and the bottom line to the highest $k_B T/\epsilon$ (0.08, 0.07, 0.06, respectively) with lines separated by $k_B \delta T/\epsilon = 0.001$. In all the panels m_σ^{min} increases when T decreases, being 0 at the higher temperatures and $\simeq 0.9$ at the lowest temperature. The value $m_\sigma = 0$ corresponds to the absence of tetrahedral order, i.e. to the high-density arrangement of water molecules. The value $m_\sigma = 1$ corresponds to full tetrahedral order of the H bonds, i.e. to the low-density arrangement of the water molecules. At $Pv_0/\epsilon = 0.7$ (left panel), by increasing T, m_σ^{min} changes without discontinuity from $\simeq 0.9$ at $k_B T/\epsilon = 0.06$ to 0 at $k_B T/\epsilon = 0.078$, denoting a continuous change from the low-density arrangement at low T to the high-density arrangement at high T. At $Pv_0/\epsilon = 0.9$ (right panel), instead, by increasing T, m_σ^{min} changes with discontinuity from $\simeq 0.6$ at $k_B T/\epsilon = 0.051$ to 0 at $k_B T/\epsilon = 0.052$, denoting a discontinuous phase change from the low-density liquid (LDL) to the high-density liquid (HDL). The pressure $Pv_0/\epsilon = 0.8$ (center panel) is very close to the critical pressure $P_{C'}$, below which the discontinuity seen at higher P disappears.

the model under the condition of being in a homogeneous phase with $v_i = v$ for any i. Although this condition can be easily removed, the solution of the model under this condition gives good qualitative agreement with the experiments, as we will see in the following sections.

The model is defined in any dimension. However, since we assume for simplicity that any molecule can form at most four H bonds, we solve the model on a regular square lattice of cells. This choice is particularly appropriate for the study of quasi-2D water [44] between hydrophobic surfaces and is a first-order approximation to the layer of water between the surface of a protein and the surface of the frozen bulk water at low T. Of course, in this approximation the interaction with the confined surfaces is not taken into account [45]. Nevertheless, the qualitative comparison with the experiments is satisfactory. The lack of the third dimension, and the number of neighbors being limited to four, could affect properties related to the amount of free space around a molecule, such as the diffusion constant [46–48]. These properties are not considered in the analysis of the model reported here.

To further simplify the simulations, the van der Waals interaction, represented in mean field by the Hamiltonian term in equation (2), is replaced by an equivalent Lennard-Jones potential with characteristic energy $-\epsilon$ at distance $R_0 \equiv v_0^{1/d}$ and truncated with a hard-core in its minimum at R_0 [11, 42, 43]. Simulations performed with a standard Lennard-Jones potential, without truncation, show that the results are qualitatively unchanged [47].
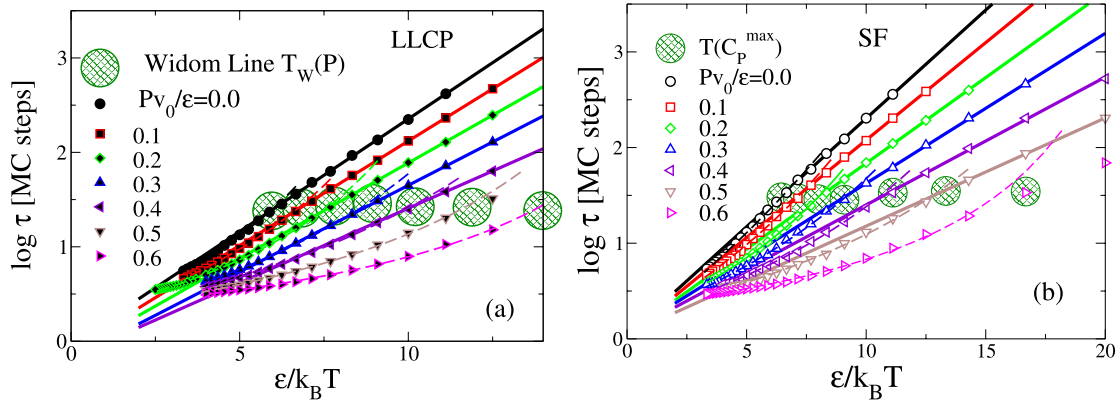
The resulting phase diagram [11] displays, at high T and low P, a gas–liquid phase transition ending in a gas–liquid critical point C. Departing from C in the supercritical region is the gas–liquid Widom line, i.e. the line of maximum—but finite—correlation length for the fluid. At lower T, the phase diagram displays the TMD line, retracing toward low T at high P as in the experiments [3]. At lower T and high P

Figure 2. The Monte Carlo phase diagram for the cell model at low T for $N = 3600$ water molecules [43]. C' is the HDL-LDL critical point, the end of first-order phase transition line (thick line) [9]; symbols are maxima of the coefficient of thermal expansion $|\alpha_P|^{max}$ (○), isobaric specific heat C_P^{max} (□), $|dp_B/dT|^{max}$ (◇) the numerical derivative of the probability of forming a H bond, proportional to the fluctuation of the number of bonds $(\delta^2 N_B)^{max}$ (△); the Widom (solid) line, corresponding to locus of maximum correlation length and estimated as the average between $|\alpha_P|^{max}$ and C_P^{max}, coincides within the error bars with $|dp_B/dT|^{max}$, i.e. with the locus of the maximum structural variation. Dashed lines are guides for the eyes.

the phase diagram displays a HDL-LDL phase transition with negative slope in the $P–T$ plane, ending in an LL critical point C'. As for the gas–liquid critical point, also from C' the line of maximum correlation length for the liquid, the LL Widom line [38, 12], departs into the one-phase region (figure 2). Therefore, the Monte Carlo results confirm the mean field analysis, displaying a phase diagram consistent with the LLCP scenario.

Recent calculations [17] show that by varying the parameters of the cell model, it is also possible to recover (i) the

Figure 3. Monte Carlo results for the dynamic crossover in the orientational relaxation time τ of the cell water model for a range of different pressures [42]. (a) In the case of the liquid–liquid critical point (LLCP) scenario, the crossover occurs at a temperature consistent with the Widom line $T_W(P)$. (b) In the case of the singularity free (SF) scenario, the crossover occurs at a temperature consistent with the $T(C_P^{max})$. In both panels the large hatched circles mark $T_W(P)$ and $T(C_P^{max})$, with a radius approximately equal to the error bar. Solid and dashed lines represent Arrhenius and Vogel–Fulcher–Tamman fits, respectively. In both cases, Kumar *et al* [42] predicted that the dynamic crossover occurs at approximately the same value of τ for all the values of pressures studied, i.e. the crossover is *isochronic*.

singularity free scenario, (ii) the stability limit scenario and (iii) the critical point free scenario. In the following we report on the analysis of the dynamics of the model for the LLCP scenario and the singularity free (SF) scenario.

6. Dynamics of the water model

We first consider the case of the LLCP scenario. Performing Monte Carlo simulations for T and P around the values of the LL Widom line $T_W(P)$, Kumar *et al* [42] found that the correlation time τ of $S_i \equiv \sum_j \sigma_{ij}/4$, which quantifies the degree of total bond ordering for site i, displays a dynamic crossover from Vogel–Fulcher–Tamman (VFT) function at high T to Arrhenius T-dependence at low T (figure 3(a)). The VFT function is given by

$$\tau^{VFT} \equiv \tau_0^{VFT} \exp\left[\frac{T_1}{T - T_0}\right], \tag{10}$$

where τ_0^{VFT}, T_1, and T_0 are three fitting parameters, and the Arrhenius function is given in equation (1). This result is qualitatively consistent with the dynamic crossover found in experiments for confined water and hydration water [23, 26, 32, 33, 36, 37] and has been related to the presence of the LLCP [38, 34].

It is, therefore, interesting to compare this result with the dynamic behavior of the cell model in the hypothesis in which the SF scenario holds. To do this, Kumar *et al* [42] analyzed the dynamics of the cell model when the H-bond correlation is zero ($J_\sigma = 0$) and the cell model recovers the SF model of Sastry *et al* [20].

The result (figure 3(b)) [42] shows that also in this scenario a dynamic crossover is expected. The temperature of the crossover coincides, within the numerical precision, with the temperature $T(C_P^{max})$ of maximum isobaric specific heat, which in the SF scenario plays a role equivalent to $T_W(P)$ of the LLCP scenario. Indeed, both $T(C_P^{max})$ and $T_W(P)$ mark

the temperature T_{struct}^{max} of the maximum structural change for the liquid [43].

The cell model allows one to clarify that the dynamic crossover is, indeed, a direct consequence of the structural change occurring at T_{struct}^{max}. By calculating, in the mean field approximation, the T-dependent activation energy $E_A(T)^{MF}$ necessary to (i) break a non-tetrahedral H bond, (ii) reorient the water molecule and (iii) form a new H bond in a tetrahedral orientation, Kumar *et al* [43] calculated the mean field correlation time as

$$\tau^{MF} = \tau_0 \exp\left[\frac{E_A(T)^{MF}}{k_B T}\right], \tag{11}$$

and compared τ^{MF} with the correlation time from the Monte Carlo simulations, finding an excellent agreement. Since E_A^{MF} is an explicit function of the number N_B of H bonds, therefore τ^{MF} is a function of the structure of the liquid [43]. Since N_B changes rapidly for $T > T_{struct}^{max}$, has its maximum variation at T_{struct}^{max}, and slowly changes for $T < T_{struct}^{max}$, the correlation time is a non-Arrhenius function of T for $T > T_{struct}^{max}$ and almost an Arrhenius function for $T < T_{struct}^{max}$, giving rise to a dynamic crossover [43]. The agreement between the mean field calculation and the Monte Carlo results clarifies that the low-T regime is only approximately Arrhenius.

The analysis of the cell model allows one, furthermore, to make a number of predictions about the dynamics of water at low T.

(i) At the dynamic crossover the value of τ is about the same for all the pressures considered in [42], i.e. the crossover is *isochronic* and the correlation time at the crossover is $\tau_L = 10^{3/2}$ in units of Monte Carlo steps [42]. Comparison with experiments, in the next section, allows one to convert this result in real time units.

(ii) The activation energy E_A, which is found by fitting the low-T dynamic regime with an Arrhenius behavior, decreases linearly for increasing P [42].

(iii) If we fix a characteristic time, for example the crossover time τ_L, the temperature T_L at which this correlation time is reached decreases linearly for increasing P [42].

All these predictions are verified in both the LLCP scenario and the SF scenario. However, Kumar *et al* [42] found a difference between the two scenarios: for the LLCP scenario the index $E_A/(k_B T_L)$ increases for increasing P, while for the SF scenario $E_A/(k_B T_L)$ is constant. However, the predicted increase of $E_A/(k_B T_L)$ is of the order of 1% [42]. As we will discuss in section 7, this increase is within the present experimental error bar.
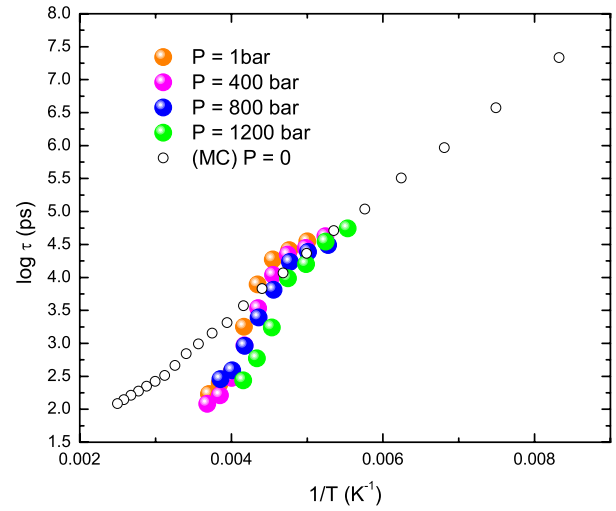
7. Comparison with the experiments on hydration water

Recently, Chen and coworkers have performed extensive QENS experiments to investigate the dynamical behavior of hydration water on lysozyme, spanning a range of pressures going from ambient pressure up to 1600 bar [51]. By measuring the mean square displacement of the of H-atoms in lysozyme, they found a dynamic crossover for all pressures studied [51]. They also found that the translational correlation time of the H-atoms of the hydration water shows a dynamic crossover for $P = 1, 400, 800, 1200, 1500$ bar [51]. For $P \leqslant 1500$ bar, they showed that the lysozyme dynamic crossover and the hydration water dynamic crossover occur at the same T [51], extending their previous results on lysozyme [23], DNA [32] and RNA [33] at ambient pressure.

They also showed that the dynamic crossover for the hydration water disappears at $P = 1600$ bar [51]. This finding, together with their previous measurements for water confined in MCM-41 Silica pore [37], suggests that the disappearance of the non-Arrhenius to Arrhenius crossover at $P = 1600$ bar is independent of the constraint used to avoid homogeneous ice nucleation. As shown in [38], the disappearance of the crossover could be the consequence of the LLCP occurring at a pressure between 1500 and 1600 bar.

The comparison of the experimental data in [51] with the results of the Monte Carlo simulations allows several observations.
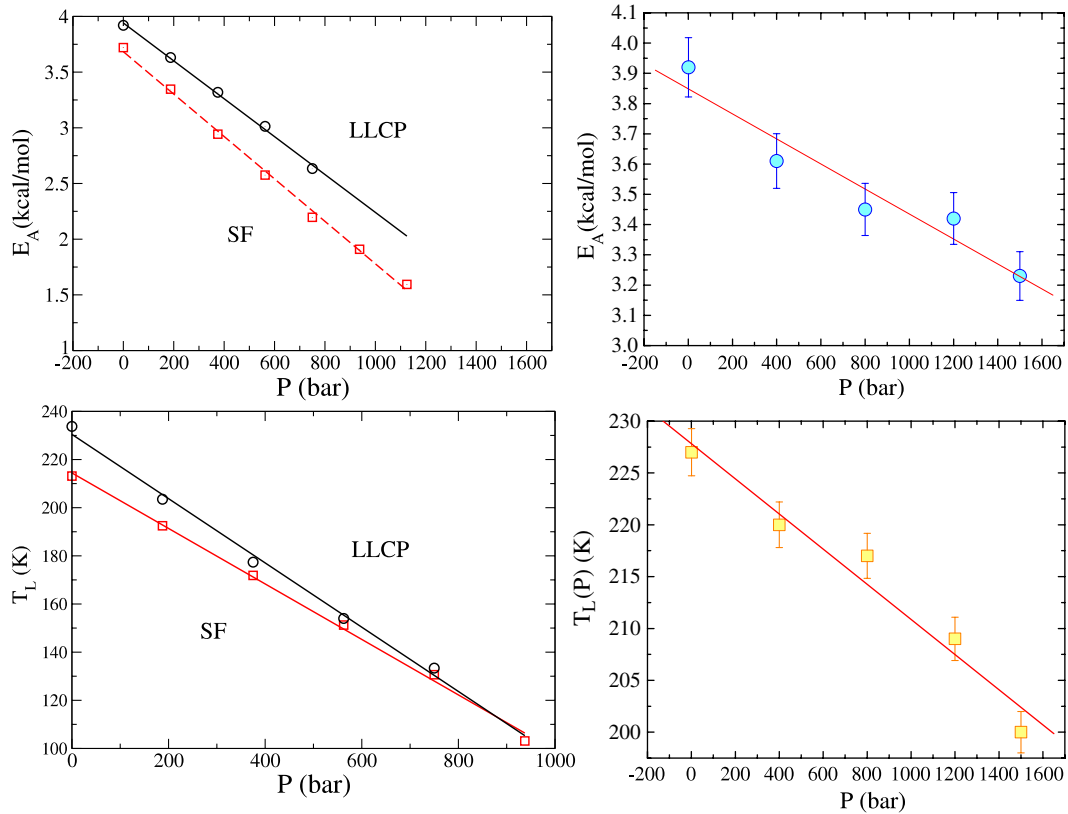
- The correlation time τ_L at the crossover is constant as predicted by the cell model, point (i) in the previous section.
- $\tau_L = 10^{3/2}$ in units of Monte Carlo steps (MCS) [42] corresponds to $10^{4.25}$ ps, i.e. 1 MCS ≈ 600 ps (figure 4).
- The high-T (non-Arrhenius) behavior of the correlation time in real water has a stronger dependence on T than the one seen in the cell model at $P = 0$ (figure 4) and is more similar to the behavior seen in the model at higher P. Since in the model this behavior is regulated by the increasing number N_B of H bonds for decreasing T, this observation implies that in real water N_B rapidly increases approaching the temperature of maximum structural change $T_{\text{struct}}^{\max}$, and N_B is smaller in real water than in the model for $T > T_{\text{struct}}^{\max}$ [43].

Figure 4. Comparison between the Monte Carlo [42] results and the QENS data [51] for the correlation time τ of supercooled water. Monte Carlo results (open symbols) are for $P = 0$ and are rescaled in such a way that the crossover occurs at the same T and τ as the experimental data (full symbols). The experimental data are for pressures going from ambient to 1200 bar.

- The low-T (approximately Arrhenius) behavior is well reproduced by the cell model (figure 4). This result implies that the estimate of the activation energy at $P = 0$ in the model compares with reasonable agreement to the activation energy measured for hydration water.
- The direct comparison of the Monte Carlo estimated activation energy E_A and the QENS data (figure 5, upper panels) shows that prediction (ii) of the previous section is verified in the experiments, with E_A decreasing linearly for increasing P. The agreement is only qualitative, since the variation of E_A in the cell model is too large with respect to the experiments.
- The crossover temperature $k_B T_L$ in the experiments verifies prediction (iii) of the cell model, i.e. $k_B T_L$ decreases linearly for increasing P (figure 5, lower panels). Also in this case, the variation in the model is too large and the agreement is only qualitative.
- The crossover temperature $k_B T_L/\epsilon \simeq 0.16$ at ambient pressure corresponds to 220 K (figure 4), leading to a van der Waals interaction strength (isotropic component of total attraction and repulsion) $\epsilon \simeq 11$ kJ mol^{-1} and a directional component of the H-bond strength $J = 0.5\epsilon = 5.5$ kJ mol^{-1}. This directional H-bond strength is about 1/4 of the total H-bond strength expected below $100\,^\circ$C [52] and is about the value estimated for the van der Waals attraction based on isoelectronic molecules at optimal separation [53].

We finally observe that the prediction of the model about the different behavior of the index $E_A/(k_B T_L)$ in the two scenarios cannot be verified in the experiments, since the predicted difference between the two scenarios (of the order of 1%) is within the error bars of the measurements [51]. The QENS data in [51] show a non-monotonic behavior for this index within an error bar larger than the 1% variation

Figure 5. Monte Carlo [42] results and the QENS data [51] for the activation energy E_A of the low-T regime and the crossover temperature T_L, as functions of the pressure P. Upper left panel: Monte Carlo results for E_A [42]; for sake of comparison with the experimental data, pressure is rescaled by an arbitrary factor 1500 bar/$(0.8\epsilon/v_0)$ and energy by a factor 16.4 kcal mol$^{-1}/\epsilon \simeq 68.7$ kJ mol$^{-1}/\epsilon$; both the liquid–liquid critical point (LLCP) scenario results (circles) and the singularity free (SF) scenario results (squares) are reported. Lower left panel: Monte Carlo results for the crossover temperature T_L; pressure is rescaled as above and temperature is rescaled by a factor 220 K/$(0.16\epsilon/k_B)$; symbols are as in the previous panel. Upper right panel and lower right panel: QENS data for the lysozyme hydration water [51].

predicted for the LLCP scenario. Hence, the data could also be considered constant within the error bars, as predicted for the SF scenario. Therefore, it is not possible to discriminate between the two scenarios on the basis of the present data for the index $E_A/(k_B T_L)$.

8. Discussion and conclusions

Several questions remain open. The work reported here allows us to propose possible answers to some of these questions.

- *Why does water have anomalies?*
  Simulations [6] first and, later, experiments [13] have shown the existence of two local configurations for water molecules: tetrahedral up to the second shell (or open) and non-tetrahedral (or closed). These local arrangements are the consequence of the orientational character of the H bonds and their typical competition between attraction and repulsion. Many of the anomalies can be understood on the basis of the tendency of the H bond to form open configurations to minimize the energy, frustrated by the necessity of reducing the occupied volume at high density or pressure.

- *What are the implications of these open and closed configurations?*
  The cell model discussed here [9–12] shows that the existence of these local configurations, related to the tendency of the H bonds to correlate and order in a tetrahedral way, is enough to imply the occurrence of a liquid–liquid phase transition, possibly ending in a critical point. Only in the hypothesis that the H bonds formed by the same molecule are completely uncorrelated, as in the Sastry *et al* model [20], do the open and closed configurations not separate into two phases, giving rise to the singularity free scenario.

- *Why is there a dynamic crossover in the correlation time of supercooled water?*
  Experiments [23] and simulations [38] offer evidence that the dynamic crossover is due to the local variation of the H-bond network [34]. The cell model discussed here, furthermore, offers an analytic relation, based on a mean field approximation, between the dynamic crossover and the structural change [42, 12]. In the cell model it is assumed that the relevant mechanism for the low-T water dynamics is the breaking of the H bonds to reorient the molecule and form more tetrahedral bonds, as seen in simulations and experiments [54].

- *Why is the dynamic crossover at the locus* $T(C_P^{\max})$ *of maximum specific heat?* At $T(C_P^{\max})$, the number N_{B} of H bonds has its maximum variation. The liquid changes from the HDL-like local structure at high T to LDL-like local structure at low T. In the HDL-like regions N_{B} rapidly increases when T decreases, implying that the activation energy E_{A} for the breaking and reorientation of the H bonds increases and the behavior is non-Arrhenius [43]. In the LDL-like regions, N_{B} is almost constant with T, implying that E_{A} is approximately constant and the behavior is asymptotically Arrhenius [43].

- *Is the dynamic crossover evidence of the liquid–liquid critical point?*
  The dynamic crossover is consistent with both the liquid–liquid critical point scenario and the singularity free scenario [42]. However, in the hypothesis of the presence of a liquid–liquid critical point it is possible to rationalize the disappearance of the dynamic crossover at high pressure [37, 38, 51].

- *Is the dynamic crossover a cooperative process?* The dynamic crossover is related to the increase of the correlation length ξ in the liquid. This quantity increases for increasing P along the Widom line and diverges at the liquid–liquid critical point. Therefore, the dynamic crossover is a cooperative process at the liquid–liquid critical point.

- *How pressure studies can help us in understanding the physics of water?*
  The recent experiments on protein hydration water [51] show that is possible to analyze the dynamic crossover of water at very low T, measuring quantities, such as the crossover temperature T_{L} and the activation energy E_{A}, whose behaviors have been predicted by the theory [42]. The experiments have verified three of the four theoretical predictions, the fourth being within the error bars.

In conclusion, in this report we compare the predictions of a cell model for water analyzed by MC in 2D [42] with the QENS data for water at the surface of lysozyme [51]. The data show a dynamic crossover from high-T non-Arrhenius behavior to low-T quasi-Arrhenius behavior for the water relaxation time at $P < 1600$ bar. Both the temperature $T_{\mathrm{L}}(P)$ and the low-T average activation energy $E_{\mathrm{A}}(P)$ linearly decrease for increasing P, as predicted by the model. The relaxation time at the crossover $\tau(T_{\mathrm{L}})$ is independent of P, as in the model. It is an open question if this isochronic behavior is related to the constant-time dynamic crossover observed in glass formers [55].

The mean field approach [42, 43] allows one to find a functional relation between E_{A} and the number $N_{\mathrm{B}}(T, P)$ of H bonds, i.e. allows one to show in a clear way that the dynamic crossover is a consequence of the structural changes occurring at the temperature of maximum specific heat $T(C_P^{\max})$. However, the comparison with the experiments does not clarify which scenario better describes the supercooled region of water. Indeed, within the experimental error bar larger than 1%, both the SF and the LLCP scenario could be consistent.

References

[1] Kumar P, Franzese G, Buldyrev S V and Stanley H E 2008 *Aspects of Physical Biology: Biological Water, Protein Solutions, Transport and Replication* ed G Franzese and M Rubi (Berlin: Springer) p 3
Swenson J, Jansson H and Bergman R 2008 *Aspects of Physical Biology: Biological Water, Protein Solutions, Transport and Replication* ed G Franzese and M Rubi (Berlin: Springer) p 23
Bresme F and Wynveen A 2008 *Aspects of Physical Biology: Biological Water, Protein Solutions, Transport and Replication* ed G Franzese and M Rubi (Berlin: Springer) p 43
Debenedetti P G and Stanley H E 2003 *Phys. Today* **56** 40
[2] Angell C A, Shuppert J and Tucker J C 1973 *J. Phys. Chem.* **77** 3092
Speedy R J and Angell C A 1976 *J. Chem. Phys.* **65** 851
[3] Debenedetti P G 1996 *Metastable Liquids: Concepts and Principles* (Princeton, NJ: Princeton University Press)
[4] Cwilong B M 1947 *Proc. R. Soc.* A **190** 137
[5] Kanno H, Speedy R J and Angell C A 1975 *Science* **189** 881
[6] Poole P H, Sciortino F, Essmann U and Stanley H E 1992 *Nature* **360** 324
Poole P H, Sciortino F, Essmann U and Stanley H E 1993 *Phys. Rev.* E **48** 3799
Poole P H, Essmann U, Sciortino F and Stanley H E 1993 *Phys. Rev.* E **48** 4605
[7] Brovchenko I, Geiger A and Oleinikova A 2003 *J. Chem. Phys.* **118** 9473
Brovchenko I, Geiger A and Oleinikova A 2005 *J. Chem. Phys.* **123** 044515
[8] Poole P H *et al* 1994 *Phys. Rev. Lett.* **73** 1632
[9] Franzese G and Stanley H E 2002 *J. Phys.: Condens. Matter* **14** 2201
[10] Franzese G and Stanley H E 2002 *Physica* A **314** 508
[11] Franzese G, Marqués M I and Stanley H E 2003 *Phys. Rev.* E **67** 011103
[12] Franzese G and Stanley H E 2007 *J. Phys.: Condens. Matter* **19** 205126
[13] Soper A K and Ricci M A 2000 *Phys. Rev. Lett.* **84** 2881
[14] Bosio L, Chen S-H and Teixeira J 1983 *Phys. Rev.* A **27** 1468
[15] Ricci M A, Bruni F and Giuliani A 2009 Similarities between confined and supercooled water *Faraday Discuss.* at press (doi:10.1039/b805706k)
[16] Angell C A 2008 *Science* **319** 582
[17] Stokely K, Mazza M G, Stanley H E and Franzese G 2008 Effect of hydrogen bond cooperativity on the behavior of water arXiv:0805.3468
[18] Speedy R J 1982 *J. Phys. Chem.* **86** 3002
[19] Debenedetti P G and Dantonio M C 1988 *AIChE J.* **34** 447
[20] Sastry S, Debenedetti P G, Sciortino F and Stanley H E 1996 *Phys. Rev.* E **53** 6144
Rebelo L P N, Debenedetti P G and Sastry S 1998 *J. Chem. Phys.* **109** 626
Rebelo L P N, Debenedetti P G and Sastry S 1999 *Phys. Rev.* E **59** 6348
[21] Stanley H E 1979 *J. Phys. A: Math. Gen.* **12** L329
Stanley H E and Teixeira J 1980 *J. Chem. Phys.* **73** 3404

Stanley H E, Teixeira J, Geiger A and Blumberg R L 1981 *Physica* A **106** 260

Geiger A and Stanley H E 1982 *Phys. Rev. Lett.* **49** 1749

[22] Schwegler E, Galli G and Gygi F 2000 *Phys. Rev. Lett.* **84** 2429

[23] Chen S-H, Liu L, Fratini E, Baglioni P, Faraone A and Mamontov E 2006 *Proc. Natl Acad. Sci. USA* **103** 9012

[24] Mamontov E 2005 *J. Chem. Phys.* **123** 171101

[25] Jansson H, Howells W S and Swenson J 2006 *J. Phys. Chem.* B **110** 13786

[26] Mallamace F, Broccio M, Corsaro C, Faraone A, Wanderlingh U, Liu L, Mou C Y and Chen S H 2006 *J. Chem. Phys.* **124** 161102

[27] Swenson J, Jansson H and Bergman R 2006 *Phys. Rev. Lett.* **96** 247802

[28] Lubchenko V, Wolynes P G and Frauenfelder H 2005 *J. Phys. Chem.* B **109** 7488

Fenimore P W, Frauenfelder H, McMahon B H and Young R D 2005 *Physica* A **351** 1

[29] Swenson J 2006 *Phys. Rev. Lett.* **97** 189801

Cerveny S, Colmenero J and Alegría A 2006 *Phys. Rev. Lett.* **97** 189802

[30] Chen S-H, Liu L and Faraone A 2006 *Phys. Rev. Lett.* **97** 189803

[31] Oleinikova A, Smolin N and Brovchenko I 2006 *J. Phys. Chem.* B **110** 19619

Brovchenko I, Krukau A and Oleinikova A 2006 *Phys. Rev. Lett.* **97** 137801

[32] Chen S-H *et al* 2006 *J. Chem. Phys.* **125** 171103

[33] Chu X, Fratini E, Baglioni P, Faraone A and Chen S-H 2008 *Phys. Rev.* E **77** 011908

[34] Kumar P, Yan Z, Xu L, Mazza M G, Buldyrev S V, Chen S-H, Sastry S and Stanley H E 2006 *Phys. Rev. Lett.* **97** 177802

[35] Errington J R and Debenedetti P D 2001 *Nature* **409** 318

[36] Faraone A, Liu L, Mou C Y, Yen C W and Chen S H 2004 *J. Chem. Phys.* **121** 10843

[37] Liu L, Chen S H, Faraone A, Yen C W and Mou C Y 2005 *Phys. Rev. Lett.* **95** 117802

[38] Xu L, Kumar P, Buldyrev S V, Chen S-H, Poole P H, Sciortino F and Stanley H E 2005 *Proc. Natl Acad. Sci. USA* **102** 16558

Xu L, Ehrenberg I, Buldyrev S V and Stanley H E 2006 *J. Phys.: Condens. Matter* **18** S2239

Xu L, Buldyrev S V, Angell C A and Stanley H E 2006 *Phys. Rev.* E **74** 031108

Xu L, Buldyrev S V, Giovambattista N, Angell C A and Stanley H E 2008 *J. Chem. Phys.* submitted

[39] D'Arrigo G, Maisano G, Mallamace F, Migliardo P and Wanderlingh F 1981 *J. Chem. Phys.* **75** 4264

[40] Angell C A and Rodgers V 1984 *J. Chem. Phys.* **80** 6245

[41] Raiteri P, Laio A and Parrinello M 2004 *Phys. Rev. Lett.* **93** 087801

[42] Kumar P, Franzese G and Stanley H E 2008 *Phys. Rev. Lett.* **100** 105701

[43] Kumar P, Franzese G and Stanley H E 2008 *J. Phys.: Condens. Matter* **20** 244114

[44] Kumar P, Buldyrev S V, Starr F W, Giovambattista N and Stanley H E 2005 *Phys. Rev.* E **72** 051503

[45] Kumar P, Starr F W, Buldyrev S V and Stanley H E 2007 *Phys. Rev.* E **75** 011202

[46] Girardi M, Szortyka M and Barbosa M C 2007 *Physica* A **386** 692

[47] de los Santos F and Franzese G 2008 in preparation

[48] Han S, Kumar P and Stanley H E 2008 *Phys. Rev.* E **77** 030201

[49] Angell C A, Borick S and Grabow M 1996 *J. Non-Cryst. Solids* **207** 463

[50] Poole P H, Hemmati M and Angell C A 1997 *Phys. Rev. Lett.* **79** 2281

[51] Chu X-Q, Faraone A, Kim C, Fratini E, Baglioni P, Leao J B and Chen S-H 2008 Pressure dependence of the dynamic crossover temperatures in protein and its hydration water arXiv:0810.1228

[52] Khan A 2000 *J. Phys. Chem.* **104** 11268

[53] Henry M 2002 *ChemPhysChem* **3** 561

[54] Laage D and Hynes J T 2006 *Science* **311** 832

Tokmakoff A 2007 *Science* **317** 54

[55] Casalini R, Paluch M and Roland C M 2003 *J. Chem. Phys.* **118** 5701

Casalini R and Roland C M 2005 *Phys. Rev.* B **71** 014210